

The Stochastic Siren: Astrophysical Gravitational-Wave Background Measurements of the Hubble Constant

BRYCE COUSINS ^{1,2} KRISTEN SCHUMACHER ^{1,2} ADRIAN KA-WAI CHUNG ^{1,2} COLM TALBOT,³ THOMAS CALLISTER,³
DANIEL E. HOLZ ^{3,4,5,6} AND NICOLÁS YUNES^{1,2}

¹*Department of Physics, University of Illinois Urbana-Champaign, Urbana, IL 61801, USA.*

²*Illinois Center for Advanced Studies of the Universe, University of Illinois Urbana-Champaign, Urbana, IL 61801, USA.*

³*Kavli Institute for Cosmological Physics, The University of Chicago, Chicago, IL 60637, USA.*

⁴*Department of Physics, University of Chicago, Chicago, IL 60637, USA.*

⁵*Department of Astronomy & Astrophysics, The University of Chicago, Chicago, IL 60637, USA.*

⁶*Enrico Fermi Institute, The University of Chicago, Chicago, IL 60637, USA.*

ABSTRACT

Gravitational waves from individually resolved compact object mergers can be used as standard sirens, offering a novel self-calibrating precision probe of cosmology. While the standard siren method has been well-explored, the gravitational-wave background arising from unresolved mergers offers a novel alternative to probing cosmology. We demonstrate that the combination of resolved binary black hole mergers with the unresolved signals composing the stochastic gravitational-wave background can be used to measure cosmological parameters, including the Hubble constant, H_0 . We apply this “stochastic siren” method to existing gravitational-wave data and find that including the current non-detection of the background increases the accuracy at which H_0 can be measured, relative to using resolved mergers alone. We also provide projections for upcoming detectors to highlight their ability to probe cosmology with the background. With the anticipated detection of the astrophysical gravitational-wave background, the stochastic siren approach can be expected to improve future standard siren cosmological measurements.

1. INTRODUCTION

While it has been known for over two decades that the Universe is undergoing an accelerating expansion (Riess et al. 1998), there are significant discrepancies in the measured expansion rate. In particular, the early- (Aghanim et al. 2020) and late-universe (Kamionkowski & Riess 2022; Di Valentino et al. 2021) measurements of the present-day expansion rate (the Hubble constant, H_0) are in $> 5\sigma$ conflict (Kamionkowski & Riess 2022), now named the Hubble tension. Late-universe probes [e.g. type Ia supernovae and the cosmic distance ladder (Riess et al. 2019; Brout et al. 2022; Freedman 2021), gravitationally-lensed systems (Suyu et al. 2010; Wong et al. 2020), and cosmic chronometers (Jimenez et al. 2019)] suggest higher values of H_0 ($\sim 70 - 72 \text{ km s}^{-1} \text{ Mpc}^{-1}$), while early-universe probes [e.g. the cosmic microwave background (Aghanim et al.

2020; Balkenhol et al. 2023), baryon acoustic oscillations (Alam et al. 2021; Collaboration et al. 2024), the inverse distance ladder (Macaulay et al. 2019)] suggest lower values ($\sim 67 - 68 \text{ km s}^{-1} \text{ Mpc}^{-1}$).

More recently, the detection of gravitational waves (GWs) enabled by the network of LIGO (Aasi et al. 2015), Virgo (Acernese et al. 2014), and KAGRA (Somiya & Collaboration 2012) detectors is offering a variety of unique methods to study the Hubble tension. Most are centered on the fact that the GWs emitted during a merger provides a direct measurement of its distance, so only a measurement of the merger’s redshift is required to compute H_0 . When an electromagnetic counterpart or host of the merger is observed and yields an independent measurement of redshift, this approach to infer H_0 is known as the “standard siren” method (Schutz 1986; Holz & Hughes 2005; Dalal et al. 2006; Nissanke et al. 2013; Vitale & Chen 2018), which has been fruitfully applied to current observations (Abbott et al. 2017; Chen et al. 2022). Other methods to obtain the redshift include using galaxy catalogs to provide a statistical redshift of the merger (Schutz 1986; MacLeod

& Hogan 2008; Del Pozzo 2012; Nishizawa 2017; Chen et al. 2018; Nair et al. 2018; Fishbach et al. 2019; Soares-Santos et al. 2019; Gray et al. 2020; Yu et al. 2020; Palmese et al. 2020; Borhanian et al. 2020; Finke et al. 2021; Abbott et al. 2023a; Gray et al. 2023), correlating galaxy distributions with merger events (Oguri 2016; Bera et al. 2020; Mukherjee et al. 2020, 2021, 2024), and using the tidal deformability of neutron stars (Messenger & Read 2012; Chatterjee et al. 2021).

Furthermore, features in the mass spectrum of mergers have been utilized in the “spectral siren” approach to break the mass-redshift degeneracy (Chernoff & Finn 1993; Taylor et al. 2012; Taylor & Gair 2012; Farr et al. 2019; You et al. 2021; Ezquiaga & Holz 2021, 2022; Mali & Essick 2025), which provides a measurement of H_0 using only GW information. The most recent spectral siren analysis from the LIGO-Virgo-KAGRA (LVK) collaboration of this nature (Abbott et al. 2023a) uses 42 binary black hole (BBH) candidates to measure $H_0 = 67_{-47}^{+91} \text{ km s}^{-1} \text{ Mpc}^{-1}$ (maximum a-posteriori probability and 90% credible interval). These results were obtained using the third GW transient catalog (GWTC-3), which are expected to improve given the hundreds of additional observations expected from the LVK and its ongoing fourth observing run O4.

In addition to individually-observed mergers, the LVK collaboration searches for the GW background (GWB) arising from unresolved signals (Abbott et al. 2016a, 2021a, 2023b). The GWB is thought to be dominated by distant compact binary mergers that cannot be individually detected (Rosado 2011; Zhu et al. 2011; Marassi et al. 2011; Abbott et al. 2021a), but it may also contain contributions from other astrophysical sources and/or early-universe phenomena (Starobinskii 1979; Kibble 1976; Easther & Lim 2006; Caprini & Figueroa 2018). While there has been a recent possible detection of a GWB produced from supermassive BBHs using pulsar timing arrays (Agazie et al. 2023), the stochastic astrophysical GWB composed of stellar-mass mergers has not yet been detected (Abbott et al. 2021a). However, given that this GWB is composed of individual merger events, its non-detection can already be used to constrain models of the BBH population (Callister et al. 2020; Abbott et al. 2021a; Turbang et al. 2024).

The astrophysical GWB can also contribute to the measurement of H_0 . Briefly, a GWB is typically characterized by Ω_{gw} , the Universe’s current energy density in GWs. This energy density is a function both of the total number of binary mergers integrated over cosmic time and, critically, the available volume over which they are distributed. Thus, the overall amplitude of the astrophysical GWB is affected by the Universe’s expan-

sion history in a unique manner not found in other H_0 measurement methods. Additionally, as recently recognized in Ferraiuolo et al. (2025), the GWB can inform constraints on population parameters which in turn can improve measurements of H_0 by breaking degeneracies; this is expected to become a powerful tool during the LVK’s O5 observing run.

In this work, we introduce the idea of leveraging the BBH GWB together with the detection of individually resolved BBH mergers to improve the measurement of H_0 , an idea we name “the stochastic siren.” We then apply this method to data from the three LVK observing runs, showing that even the current non-detection of the GWB can inform measurements of H_0 . This is possible because a larger Hubble constant implies a smaller amplitude of the GWB, and thus a non-detection of the GWB can exclude lower values of H_0 . By combining and synthesizing information from BBH population inference and the search for the GWB, we improve the accuracy of the Hubble constant measurement relative to BBH-only methods.

The remainder of this paper presents the details of the stochastic siren method and our implementation. Section 2 reviews the dependence of the GWB energy spectrum on H_0 and the likelihood of observing a stochastic background and individual mergers, given values of population and cosmological parameters. Section 3 outlines the stochastic siren method and combines the LVK’s GWTC-3 population results (Abbott et al. 2023c) with the GWTC-3 GWB constraints (Abbott et al. 2021b) to obtain a measurement of H_0 . Section 4 reviews our work and discusses how it could be applied and extended for future work.

Throughout this paper, we refer to the resolved BBHs as “FG” (foreground) signals and unresolved BBHs as “BG” (background) signals. We use “GWB” to refer to the stochastic astrophysical background arising from stellar-mass BBH mergers, unless otherwise noted. We assume a flat cosmology ($\Omega_k = 0$) as is standard given previous results (Aghanim et al. 2020), but allow the other cosmological energy densities and H_0 to vary during cosmological inference. We provide several Appendices to further define and derive quantities discussed in the main text, as well as to elaborate on our results and provide forecasts for GWB detection in various cosmologies.

2. THEORY AND ANALYSIS FORMALISM

2.1. GWB dependence on the Hubble constant

The general form of the GWB spectral energy density is the dimensionless amplitude

$$\Omega_{\text{gw}}(f) = \frac{f}{\rho_c c^2} \frac{d\rho_{\text{gw}}}{df}, \quad (1)$$

where c is the speed of light, f is the observer frame frequency, $\rho_c \equiv 3H_0^2/8\pi G$ is the critical mass density of the Universe (with gravitational constant G), and $d\rho_{\text{gw}}$ is the energy density in the frequency interval $(f, f+df)$ in the observer frame (Allen & Romano 1999; Ferrari et al. 1999a; Romano & Cornish 2017).

Compact binary mergers will contribute to Ω_{gw} based on their source properties ϕ (e.g., the spins and masses of the components) and their merger rate density $\mathcal{R}(z)$ (number per comoving volume per unit time in the source frame). In this case, $d\rho_{\text{gw}}$ can be expressed as a redshift integral across the mergers (Ferrari et al. 1999a; Regimbau & Mandic 2008; Regimbau 2011), so

$$\Omega_{\text{gw}} = \frac{8\pi G}{3c^2 H_0^3} f \int_0^{z_{\text{max}}} \frac{\mathcal{R}(z)}{(1+z)E(z)} \left\langle \frac{dE_{\text{gw}}}{df_s} \right\rangle_{f_s} dz, \quad (2)$$

where $E(z)$ is a dimensionless function of redshift, cosmological energy densities, and dark energy as elaborated in App. A.2. The bracketed quantity in Eq. (2) is the average energy spectrum of a single binary evaluated at the source frame frequency $f_s = f(1+z)$:

$$\left\langle \frac{dE_{\text{gw}}}{df_s} \right\rangle_{f_s} = \int d\phi p(\phi) \frac{dE_{\text{gw}}(\phi, f_s)}{df_s} \quad (3)$$

Note that there is direct dependence on H_0 in Eq. (2): $\Omega_{\text{gw}} \sim H_0^{-3}$. In App. A.3, we provide a detailed derivation of Ω_{gw} and this dependence on H_0 and other quantities. We show there that the H_0 dependence is ultimately due to $\mathcal{R}(z)$ and its association with the comoving volume.

A major implication of this dependence is that Ω_{gw} is sensitive to the acceleration of the Universe, as follows. The value of H_0 is inversely-proportional to the comoving distance between points in space at a given redshift (see Hogg (1999) and standard texts, e.g., Dodelson & Schmidt (2003)). A higher value of H_0 would hence cause distances to be smaller, meaning that fewer mergers would be encompassed in any given comoving volume of space under a fixed merger rate density. Therefore, a universe with a higher value of H_0 would possess fewer mergers contributing to the GW energy density, leading to a smaller, harder-to-detect GWB signal. The inverse is also true, meaning that ruling out higher values of Ω_{gw} would correspondingly rule out lower values of H_0 . Thus, even with the current non-detection of the GWB, it is possible to inform measurements of H_0 using the GWB as a ‘‘stochastic siren.’’

2.2. Likelihood probability distributions

GW observations follow an inhomogeneous Poisson distribution characterized by the differential merger rate of binaries $R_\phi(\phi|\vec{\lambda}, R) = R p(\phi|\vec{\lambda})$, where $\vec{\lambda}$ refers to population model hyperparameters and $p(\phi|\vec{\lambda})$ is the probability of an event having source parameters ϕ . The quantity R is the total number of mergers throughout the Universe per unit observer-frame time. Taking the fraction of astrophysical sources that are observable as $P_{\text{det}}(\vec{\lambda})$, the likelihood of observing a catalog of foreground GW events is given by (Taylor & Gerosa 2018; Mandel et al. 2019; Vitale et al. 2022)

$$\mathcal{L}_{\text{FG}}(\{d\}|\vec{\lambda}, H_0) \propto N^{N_{\text{obs}}} e^{-NP_{\text{det}}(\vec{\lambda}, H_0)} \prod_{i=1}^{N_{\text{obs}}} \mathcal{L}(d_i|\vec{\lambda}, H_0) \quad (4)$$

where $N = RT$ is the total number of mergers occurring during observing time T , and the per-event likelihood terms are generally calculated by explicitly marginalizing over all possible signals assuming Gaussian detector noise. We emphasize that we use a formulation of the foreground likelihood with explicit rate dependence because the rate is also explicitly required in the background likelihood.

Searches for the unresolved background of compact binary mergers typically assume the signal is stationary, Gaussian, unpolarized, and isotropic, although see Drasco & Flanagan (2003); Smith & Thrane (2018) for alternative approaches. Such a GWB can be searched for by cross-correlating the strain measured by different pairs of detectors within the LVK network. Following Allen & Romano (1999) and Romano & Cornish (2017), for a baseline comprising the detectors I and J , we define the following cross-correlation statistic,

$$\hat{C}(f) = \frac{1}{\Delta t} \frac{20\pi^2}{3H_0^2} f^3 \tilde{s}_I(f) \tilde{s}_J^*(f), \quad (5)$$

where $\tilde{s}_I(f)$ and $\tilde{s}_J(f)$ are respectively the short-time Fourier transform of the strain measured by the detectors I and J , and Δt is the segment time length. The background likelihood (\mathcal{L}_{BG}) of observing this cross-correlation statistic for the background given some $\vec{\lambda}$ is well approximated by a Gaussian (Mandic et al. 2012; Callister et al. 2017, 2020):

$$\mathcal{L}_{\text{BG}}(\hat{C}|\vec{\lambda}, H_0) \propto \exp \left[-\frac{1}{2} \left(\hat{C} - \gamma \Omega_{\text{gw}}(\vec{\lambda}, H_0) \right) \left(\hat{C} - \gamma \Omega_{\text{gw}}(\vec{\lambda}, H_0) \right) \right], \quad (6)$$

where $\gamma(f)$ is the overlap reduction function that gives the sensitivity of a particular pair of detectors to an

Parameter	Description	Prior
<i>Mass model parameters</i>		
α	Index of power law primary mass	$\mathcal{U}(1.5, 12)$
β	Index of power law secondary mass	$\mathcal{U}(-4, 12)$
m_{min}	Minimum mass	$\mathcal{U}(2M_{\odot}, 10M_{\odot})$
m_{max}	Maximum mass	$\mathcal{U}(50M_{\odot}, 200M_{\odot})$
λ_g	Fraction of events in Gaussian	$\mathcal{U}(0, 1)$
μ_g	Peak of Gaussian	$\mathcal{U}(20M_{\odot}, 50M_{\odot})$
σ_g	Width of Gaussian	$\mathcal{U}(0.4M_{\odot}, 10M_{\odot})$
δ_m	Range of tapering function	$\mathcal{U}(0M_{\odot}, 10M_{\odot})$
<i>Population hyperparameters</i>		
R_0	The BBH merger rate at $z = 0$	$\mathcal{U}(0, 100)$
γ	Index for the power law before z_p	$\mathcal{U}(0, 12)$
κ	Index for the power law after z_p	$\mathcal{U}(0, 6)$
z_p	Peak redshift	$\mathcal{U}(0, 4)$
<i>Cosmological parameters</i>		
$\Omega_{m,0}$	Present matter energy density	$\mathcal{U}(0, 1)$
w_0	Dark energy equation of state parameter	$\mathcal{U}(-3, 0)$
H_0	Hubble constant	$\mathcal{U}(10, 200)$

Table 1. A summary of the parameters considered and the uniform priors \mathcal{U} used for parameter inference. The mass model is the **PowerLaw+Peak** model (Talbot & Thrane 2018; Collaboration et al. 2019; Talbot et al. 2024) with eight parameters. The population model follows (Madau & Dickinson 2014) and gives us four more parameters, for a total of 12 astrophysical population parameters. The addition of the three cosmological parameters brings the total to 15 parameters.

isotropic background based on their relative geometry (Christensen 1992; Flanagan 1993; Allen & Romano 1999). The inner product in this likelihood is conventionally defined as

$$(A|B) = 2T \left(\frac{3H_0^2}{10\pi^2} \right)^2 \int_0^\infty df \frac{\tilde{A}(f)\tilde{B}^*(f)}{f^6 P_I(f)P_J(f)} \quad (7)$$

with $P_I(f)$ the one-sided noise PSD of detector I . Note that this likelihood depends on H_0 through the inner product, the cross-correlation statistic, and the energy density of the GWB.

Following Callister et al. (2020), we assume the data contributing to the foreground and background terms are independent. In practice, there will be some cross-contamination due to the observed mergers contributing to the “background” signal unless they are explicitly removed. However, we expect this effect to be a small correction; individually-resolved compact binaries detected during the O3 observing run, for example, are expected to contribute to the GWB only at $\Omega_{\text{gw}} \lesssim 10^{-10}$, well below current upper limits. Thus, the full joint likelihood is simply the product

$$\mathcal{L}_{\text{joint}} = \mathcal{L}_{\text{FG}}\mathcal{L}_{\text{BG}}. \quad (8)$$

3. DATA ANALYSIS AND RESULTS

In order to apply the stochastic siren method to GW data, the rate density $\mathcal{R}(z)$ in Eq. (2) and the source energy spectrum within Eq. (3) must be computed to obtain a value of Ω_{gw} . We address these using

parametrized models for the source redshift and component mass distributions, which involve 12 hyperparameters (described in Table 1).

In this current work, we exclusively consider BBHs given that their population properties are better understood than those of binary neutron stars or neutron star / black hole mergers (Abbott et al. 2023b), which will result in an underestimate of Ω_{gw} and hence conservative bounds on H_0 . We assume that the individual BBH energy spectra follow the Newtonian limit of an inspiralling circular binary with source-frame masses m_1 and m_2 (as in, e.g., Thorne (1987)):

$$\frac{dE_{\text{gw}}}{df_s} = \frac{(\pi G)^{2/3}}{3f_s^{1/3}} \frac{m_1 m_2}{(m_1 + m_2)^{1/3}} \quad (9)$$

To model $\mathcal{R}(z)$, we follow Callister et al. (2020) and fit the redshift distribution of merging binaries with a functional form of the Madau-Dickinson star formation rate (Madau & Dickinson 2014). This four-parameter model possesses a smooth transition between two power-law distributions with a peak at redshift z_p and a local merger rate density ¹ $R_0 = \mathcal{R}(z = 0)$, fully described in App. C.1 as Eq. (C26).

As motivated by current observations (Collaboration et al. 2019), we model the BBH mass distribution using the **PowerLaw+Peak** model (Talbot & Thrane 2018; Talbot et al. 2024), an eight-parameter model consisting of a truncated power-law component and a Gaussian component for the primary mass and a power-law distribution of mass ratios. Both the primary mass and mass ratio distributions are smoothly tapered at low masses.

We neglect the possibility of correlations between the astrophysical mass and redshift distributions. Some correlation between these parameters is expected due to metallicity variation of progenitor stars (Belczynski et al. 2010) and variation in the delay time of BBH formation and merger (Kushnir et al. 2016; Gallegos-Garcia et al. 2021; Van Son et al. 2022), and it may influence parameter inference (Rinaldi et al. 2024; Tornamenti et al. 2024). However, it has recently been found that such a correlation is unlikely to be relevant with the current population and may not be required by current data (Lalleman et al. 2025).

Beyond the 12 population parameters described above, we include three cosmological parameters. As in Abbott et al. (2023a), we consider H_0 , the present-day matter energy density $\Omega_{m,0}$, and one parameter for the dark energy equation of state $w(z) = w_0$ (which en-

¹ Note that $R_0 \neq R$ in Sec. 2.2, where the latter is the total merger rate density integrated over the Universe’s total volume.

ters Ω_{gw} via $E(z)$ as derived in App. A.2). This yields a total of 15 parameters for our full inference.

3.1. Likelihood analysis using GW data

To measure H_0 , we must compute each of the two likelihoods given available data. For \mathcal{L}_{FG} , we must be able to determine the likelihood of observed BBHs given $\vec{\lambda}$. For \mathcal{L}_{BG} , we must be able to compute Ω_{gw} given $\vec{\lambda}$, and then determine the associated likelihood of that value of Ω_{gw} .

To compute \mathcal{L}_{FG} , we use the hyperparameter posteriors derived with ICAROGW (Mastrogiovanni et al. 2023) for the GWTC-3 population analysis (Abbott et al. 2023b,a). These results considered BBH mergers with a signal-to-noise ratio (SNR) greater than 11. We use these posteriors to generate a 15-dimensional kernel density estimator (KDE) to provide a function for the probability of a given $\vec{\lambda}$.

For \mathcal{L}_{BG} , we consider a power-law form of Ω_{gw} with spectral index $\alpha = 2/3$ as expected for the GWB (Regimbau 2011), with a reference frequency of 25 Hz as is typical with current GWB searches (Abbott et al. 2023b, 2021a). We note that the existing posteriors of Ω_{gw} obtained from previous searches for the GWB (Abbott et al. 2021a) can be used to compute Ω_{gw} . This is possible via Bayes’ theorem in the form

$$p_{\text{BG}}(\Omega_{\text{gw}}|\hat{C}) \propto \pi_{\text{BG}}(\Omega_{\text{gw}})\mathcal{L}_{\text{BG}}(\hat{C}|\Omega_{\text{gw}}), \quad (10)$$

where p_{BG} and π_{BG} are the posterior and prior distributions for Ω_{gw} , respectively. If we consider a uniform prior, then we can invert Eq. (10) for the likelihood,

$$\mathcal{L}_{\text{BG}}(\hat{C}|\Omega_{\text{gw}}) \propto p_{\text{BG}}(\Omega_{\text{gw}}|\hat{C}). \quad (11)$$

We obtain p_{BG} by using the posterior of $\Omega_{\alpha=2/3}$ constructed from the data obtained during the first three observing runs of the LVK detectors (Abbott et al. 2021a), under a uniform π_{BG} , which allows us to compute \mathcal{L}_{BG} . We use the posterior samples of $\Omega_{\alpha=2/3}$ to generate a 1-dimensional KDE to estimate \mathcal{L}_{BG} as a function of Ω_{gw} within the range covered by the prior of $\Omega_{\alpha=2/3}$. Then, since Ω_{gw} is just a function of $\vec{\lambda}$, we are able to evaluate \mathcal{L}_{BG} as a function of population and cosmological parameters.

These two individual likelihoods, \mathcal{L}_{BG} and \mathcal{L}_{FG} , together compose the joint likelihood of Eq. (8), giving a function of the 15 (hyper)parameters we consider. We then perform nested sampling (Skilling 2004, 2006) over these parameters to compute $\mathcal{L}_{\text{joint}}$ using the `dynesty` sampler (Speagle 2020), as implemented in the `bilby` package (Ashton et al. 2019). The prior distributions for our 12 astrophysical population hyperparameters and three cosmological parameters are provided in Table 1.

3.2. Stochastic siren inference of the Hubble constant

We present the results of the stochastic siren method for current GWTC-3 data in Fig. 1. In addition to the full $\mathcal{L}_{\text{joint}}$ result (red), we provide a comparison with the results obtained when considering only the foreground (\mathcal{L}_{FG} , blue) and background (\mathcal{L}_{BG} , orange) populations. Since a uniform prior is prescribed for the population-model hyperparameters and cosmological parameters (c.f. Tab. 1), all likelihood distributions are proportional to the corresponding posterior probability distribution, which is a function of H_0 . Note that we show the values of H_0 as measured by Planck (Aghanim et al. 2020) and SH0ES (Riess et al. 2022), marked respectively by vertical dotted and dashed lines.

Observe that there is an improvement in the measurement accuracy of $\mathcal{L}_{\text{joint}}$ relative to \mathcal{L}_{FG} : the H_0 posteriors as obtained via $\mathcal{L}_{\text{joint}}$ peak at a value that is closer to the Hubble tension region, which indicates an improvement in the consistency between the GW and electromagnetic measurements of H_0 . This can be seen when comparing the maximum a-posteriori probability (MAP) between methods: using the mode of the H_0 posterior distribution, we find the MAP for $\mathcal{L}_{\text{joint}}$ to be 70 versus 43 for \mathcal{L}_{FG} , or compared to 46 from the spectral siren BBH-only analysis of Abbott et al. (2023a).

4. DISCUSSION

We have detailed how the combination of the resolved BBH population and the predicted BBH GWB could be used as a “stochastic siren” to measure the Hubble constant. We have shown that the GWB can provide additional information and aid in the measurement of the Hubble constant due to its dependence on cosmological parameters. When applied to the data obtained by the LVK detectors during their first three observing runs, the stochastic siren shows improvements in accuracy over both the foreground-only spectral siren and background-only method, even though the GWB has yet to be observed. We note that by considering only BBHs, we obtain conservative results because the current GWB constraints were obtained by searching for a background arising from all merger types, favoring values of Ω_{gw} that are higher than what BBHs would produce alone. Hence, lower values of Ω_{gw} are less probable, which leads to weaker constraints on higher values of H_0 .

Various extensions could be made to our exploratory study. For example, we considered only a single set of population models in this work, but the method can be easily extended to accommodate a variety of population models. Additionally, other classes of mergers are expected to contribute to the GWB at levels comparable to BBHs (Abbott et al. 2021a, 2023b). While

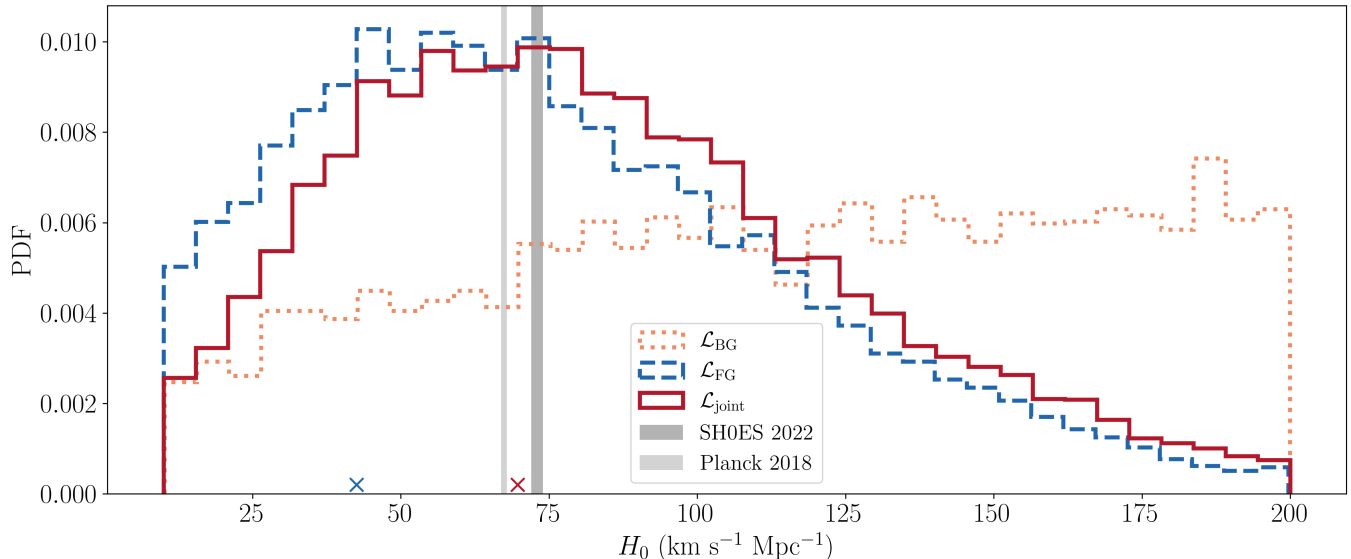


Figure 1. The posterior distributions of the Hubble constant obtained through the BBH spectral siren (\mathcal{L}_{FG} , dashed blue), the GWB search (\mathcal{L}_{BG} , dotted orange), and the stochastic siren joint measurement ($\mathcal{L}_{\text{joint}}$, red), each respectively marginalized over their 14 other parameters. Since no GWB has been detected, the background search shows less support for lower values of the Hubble constant. Combining this information with the BBH spectral siren shifts the joint posterior, as indicated by the maximum a-posteriori probabilities for \mathcal{L}_{FG} and $\mathcal{L}_{\text{joint}}$ shown here by the \times markers and discussed further in the main text. The joint measurement peaks closer to the Hubble tension region vertically demarcated by the Planck (Aghanim et al. 2020) and SH0ES (Riess et al. 2022) values, indicating improved consistency with existing measurements.

the inclusion of these other merger classes would require additional population modeling and more observations, it would enhance the stochastic siren method. Aside from compact object mergers, other GW sources, such as supernovae, could produce observable GWBs (Ferrari et al. 1999b; Chowdhury & Khlopov 2024). These contributions could also be included, but would require changing the spectral index of Ω_{gw} and performing population inference for these alternative source classes. Finally, in line with the work of Ferraiuolo et al. (2025), the proper integration of our method with existing population, stochastic, and cosmology analysis systems in the LVK (e.g., Fischbach et al. 2021; Mastrogiovanni et al. 2023; Gray et al. 2023; Renzini et al. 2023; Talbot et al. 2024; Renzini & Golomb 2024) would help improve cosmological constraints as LVK observing runs continue.

As current GWB constraints become stronger, a continued non-detection would raise the lower bound of H_0 , thereby progressively improving the precision of the stochastic-siren measurement. Moreover, the LVK detectors are expected to observe the GWB in coming years (Abbott et al. 2016b, 2018; Renzini et al. 2022), at which point the stochastic siren method would yield even stronger improvements on the measurement of H_0 . Our current projections in App. B suggest that the GWB could be detected with an SNR of eight in less than two years using the anticipated A# detector up-

grades. In these projections, we also consider a variety of different cosmological and population parameters, showing what regions of parameter space will be probed during this time by the GWB and its detection or non-detection.

The future utility of combining the BBH GWB with resolved BBHs to perform population and cosmological inference is explored more thoroughly by Ferraiuolo et al. (2025) via a full mock data analysis. Their results demonstrate that two years of observations during LVK’s O5 would improve upon the O5 foreground spectral siren H_0 measurement by more than factor of two, and that measurements of some population parameters would also improve. They also perform a re-analysis of GWTC-3 data and obtain results similar to our findings here, albeit with slightly different data (59 BBHs selected based on false-alarm rate) and inference methods (i.e., using ICAROGW for population and GWB inference, with a fixed value of w_0).

While upcoming LVK observing runs and upgrades may enable the detection of the GWB, next-generation ground-based detectors are expected to come online soon after (Punturo et al. 2010; Reitze et al. 2019; Maggiore et al. 2020; Evans et al. 2021, 2023; Branchesi et al. 2023). However, the GWBs detected by these future detectors are expected to be non-Gaussian and non-stationary (Buscicchio et al. 2023), which would

require modifications to the approach of GWB analysis we considered here. Moreover, the assumption that \mathcal{L}_{BG} and \mathcal{L}_{FG} are independent (allowing the construction of the joint likelihood in Eq. (8)) may no longer hold given the greater number of resolved mergers, warranting a more careful consideration of foreground and background sources.

The stochastic siren approach has ample room for development, but it can already inform current investigations of the Hubble tension. While the constraints obtained using only the current GWB upper limits may be less stringent when compared to other GW measurement methods, including the GWB provides an independent measure of H_0 without the need for merger redshifts or electromagnetic information. This suggests that it could be used to improve the overall results of GW H_0 measurements, as further indicated by the recent results of Ferraiuolo et al. (2025). Moreover, as searches for the GWB continue, our method has potential to serve a unique role in that the lower bound of the H_0 measurement will progressively increase in the event of continued non-detection. This will culminate with the eventual detection of the GWB and its resulting cosmological constraints, framing the stochastic siren as a promising tool for GW cosmology.

1 We thank the authors of Ferraiuolo et al. (2025) for the
 2 constructive coordination and feedback during the in-
 3 ternal LVK review of this work. B.C. acknowledges
 4 that this material is based upon work supported by
 5 the NSF Graduate Research Fellowship Program under
 6 Grant No. DGE 21-46756. K. S. would like to acknowl-
 7 edge the NSF Graduate Research Fellowship Program
 8 under Grant No. DGE-1746047 and the NSF under
 9 award PHY-2207650. A.K.W.C and N.Y. acknowledge
 10 the support from the Simons Foundation through Award
 11 No. 896696, the NSF through award PHY-2207650 and
 12 NASA through Grant No. 80NSSC22K0806. C. T. and
 13 T. C. are supported by the Eric and Wendy Schmidt
 14 AI in Science Postdoctoral Fellowship, a Schmidt Sci-
 15 ences program. D.E.H is supported by NSF grant PHY-
 16 2110507, as well as by the Kavli Institute for Cosmologi-
 17 cal Physics through an endowment from the Kavli Foun-
 18 dation and its founder Fred Kavli. This work made use
 19 of the Illinois Campus Cluster, a computing resource
 20 that is operated by the Illinois Campus Cluster Pro-
 21 gram (ICCP) in conjunction with the National Center
 22 for Supercomputing Applications (NCSA) and which is
 23 supported by funds from the University of Illinois at
 24 Urbana-Champaign. This material is based upon work
 25 supported by National Science Foundation (NSF) LIGO
 26 Laboratory, which is a major facility fully funded by the
 27 NSF.

Software: `astropy` (Astropy Collaboration et al. 2013, 2018, 2022), `h5py` (Collette 2013), `matplotlib` (Hunter 2007), `numpy` (Harris et al. 2020), `scipy` (Virtanen et al. 2020).

APPENDIX

A. COSMOLOGY AND THE GWB

A.1. *Definitions*

We first make cosmological definitions with the Hubble parameter $H(z)$:

$$H(z) = H_0 [(1+z)^3 \Omega_m + (1+z)^2 \Omega_k + \Omega_\Lambda]^{1/2}, \quad (\text{A1})$$

which allows us to obtain $E(z)$ involving the cosmological energy densities (dark energy Ω_Λ , curvature Ω_k , and matter Ω_m):

$$E(z) \equiv \frac{H(z)}{H_0} = [(1+z)^3 \Omega_m + (1+z)^2 \Omega_k + \Omega_\Lambda]^{1/2}. \quad (\text{A2})$$

In our analysis, we consider only a flat universe, so $\Omega_k = 0$, so Eq. (A2) becomes

$$E(z) \equiv \frac{H(z)}{H_0} = [(1+z)^3 \Omega_m + \Omega_\Lambda]^{1/2}. \quad (\text{A3})$$

We next define the requisite distance measures:

- Hubble distance:

$$D_H \equiv c/H_0 \quad (\text{A4})$$

- line-of-sight comoving distance:

$$D_C = \frac{c}{H_0} \int_0^z \frac{dz}{E(z)} = D_H \int_0^z \frac{dz}{E(z)} \quad (\text{A5})$$

- transverse comoving distance:

$$D_M = \begin{cases} D_H \frac{1}{\sqrt{\Omega_k}} \sinh [\sqrt{\Omega_k} D_C/D_H] & \text{for } \Omega_k > 0 \\ D_C & \text{for } \Omega_k = 0 \\ D_H \frac{1}{\sqrt{|\Omega_k|}} \sin [\sqrt{|\Omega_k|} D_C/D_H] & \text{for } \Omega_k < 0 \end{cases} \quad (\text{A6})$$

- angular diameter distance:

$$D_A = \frac{D_M}{1+z} = \frac{D_C}{1+z} \text{ when } \Omega_k = 0 \quad (\text{A7})$$

- luminosity distance:

$$D_L = (1+z)D_M = (1+z)D_C \text{ when } \Omega_k = 0 \quad (\text{A8})$$

A.2. $E(z)$ for parametrized dark energy

Using the dark energy equation-of-state parameter $w(z)$, we follow [Linder \(2003\)](#) and rewrite Eq. (A3) as

$$E(z, w, \Omega_k = 0) = \left\{ (1+z)^3 \Omega_m + \Omega_\Lambda \exp \left[-3 \int_0^{\ln(1+z)} d \ln(1+z') [1 + w(z')] \right] \right\}^{1/2}. \quad (\text{A9})$$

We note that the only term with dependence on $w(z)$ is the exponential on the right-hand side. We next modify this term using a parametrization of $w(z)$. In general, $w(z)$ can be solved for under a specific scalar field theory, or is more generically parametrized. In this work, however, we assume a constant equation of state parameter ($w(z) = w_0$, as

in [Abbott et al. \(2023a\)](#)). Then, the integral in the exponential can be solved analytically: let $y \equiv d \ln(1+z)$, so the integral becomes

$$\left[-3 \int_0^y dy(1+w_0) \right] = y(1+w_0) = \ln(1+z)(1+w_0), \quad (\text{A10})$$

which allows the exponential to be rewritten as

$$\exp[-3 \ln(1+z)(1+w_0)] = (1+z)^{-3(1+w_0)}. \quad (\text{A11})$$

Equation (A9) is then simply

$$E(z, w, \Omega_k = 0) = \left[(1+z)^3 \Omega_m + \Omega_\Lambda (1+z)^{-3(1+w_0)} \right]^{1/2}. \quad (\text{A12})$$

A.3. Derivation of the GWB energy density

We derive the GWB energy density Ω_{gw} , generally following the procedure of earlier work ([Ferrari et al. 1999a](#); [Regimbau & Mandic 2008](#); [Regimbau 2011](#); [Zhu et al. 2011](#); [Wu et al. 2012](#)) while avoiding the occasional error of incorrect cosmological distances and/or frames that can result in incorrect factors of $(1+z)$ as noted in [Zhu et al. \(2013\)](#). Note that for consistency with LVK convention, we express frequencies as f instead of the occasionally-used ν ; we hence express the fluence here as \mathcal{F} instead of f .

The dimensionless energy density Ω_{gw} for an astrophysical GWB is typically expressed as:

$$\Omega_{\text{gw}} = \frac{f}{\rho_c c^3} F(\phi, f) \quad (\text{A13})$$

where $f = f_s/(1+z)$ is the observer-frame GW frequency in terms of the source-frame frequency f_s and F is the integrated flux of the astrophysical sources:

$$F(\phi, f) = \int p(\phi) \int_0^{z_{\text{max}}} \mathcal{F}(\phi, f) \frac{d\dot{N}^\circ(\phi, z)}{dz} d\phi dz, \quad (\text{A14})$$

for source parameters ϕ and associated probability distribution $p(\phi)$, source fluence $\mathcal{F}(\phi, f)$ (flux times time), and the total number of events per unit observer time per redshift interval $d\dot{N}^\circ(\phi, z)/dz$.

We first consider the fluence, which is the energy per unit area A per unit frequency and introduce the solid angle differential $d\Omega$. We take its definition (in source frame and frequency) as Eq. (2.45) of [Flanagan & Hughes \(1998\)](#):

$$\mathcal{F}(\phi, f) \equiv \frac{dE}{dA df} = \frac{(1+z)^2}{D_L^2} \frac{dE_{\text{gw}}(\phi, f_s)}{d\Omega df_s} = \frac{(1+z)^2}{(1+z)^2 D_C^2} \frac{dE_{\text{gw}}(\phi, f_s)}{d\Omega df_s} = \frac{1}{D_C^2} \frac{dE_{\text{gw}}(\phi, f_s)}{d\Omega df_s} \quad (\text{A15})$$

where we have used the luminosity distance as defined in Eq. (A.1). Note here that the emitted gravitational spectral energy is $dE_{\text{gw}}(\phi, f)/df_s$, as used in Eq. (3).

We next consider the total number of events per unit *observer* time, per redshift interval,

$$\frac{d\dot{N}^\circ(\phi, z)}{dz} = \mathcal{R}^\circ(\phi, z) \frac{dV}{dz}(z), \quad (\text{A16})$$

for observer-frame comoving event rate density \mathcal{R}° comoving volume element

$$dV_C = D_H \frac{(1+z)^2 D_A^2}{E(z)} d\Omega dz = \frac{c}{H_0} \frac{D_C^2}{E(z)} d\Omega dz. \quad (\text{A17})$$

Combining the above two equations yields

$$\frac{d\dot{N}^\circ(\phi, z)}{dz} = \mathcal{R}^\circ(\phi, z) \frac{c}{H_0} \frac{D_C^2}{E(z)} d\Omega. \quad (\text{A18})$$

To match current literature, we next convert to *source* time. This requires redshifting to the source-frame comoving rate density $\mathcal{R} = (1+z)\mathcal{R}^\circ$ (since time redshifts as $t_s = t/(1+z)$), so we rewrite Eq. (A18) as

$$\frac{d\dot{N}^\circ(\phi, z)}{dz} = \frac{\mathcal{R}(\phi, z)}{(1+z)} \frac{c}{H_0} \frac{D_C^2}{E(z)} d\Omega. \quad (\text{A19})$$

We then assemble the integrated flux by inserting Eq. (A15) and Eq. (A19) into Eq. (A14):

$$\begin{aligned} F(\phi, f) &= \int p(\phi) d\phi \int_0^{z_{max}} \frac{1}{D_C^2} \frac{dE_{\text{gw}}(\phi, f_s)}{d\Omega df_s} \frac{\mathcal{R}(\phi, z)}{(1+z)} \frac{c}{H_0} \frac{D_C^2}{E(z)} d\Omega \\ &= \frac{c}{H_0} \int_0^{z_{max}} \frac{\mathcal{R}(z)}{(1+z)E(z)} \int p(\phi) \frac{dE_{\text{gw}}(\phi, f_s)}{df_s} d\phi dz \\ &= \frac{c}{H_0} \int_0^{z_{max}} \frac{\mathcal{R}(z)}{(1+z)E(z)} \left\langle \frac{dE_{\text{gw}}}{df_s} \right\rangle_{f_s} dz, \end{aligned} \quad (\text{A20})$$

where we obtain the second line by assuming no correlation between source parameters and redshift ($\mathcal{R}(z, \phi) = \mathcal{R}(z)$) as elaborated in Sec. 3. We obtain the third line by defining

$$\left\langle \frac{dE_{\text{gw}}}{df_s} \right\rangle_{f_s} \equiv \int p(\phi) \frac{dE_{\text{gw}}(\phi, f_s)}{df_s} d\phi. \quad (\text{A21})$$

Finally, by inserting Eq. (A20) into Eq. (A13), we find that the GW energy density is

$$\boxed{\Omega_{\text{gw}} = \frac{f}{\rho_c c^2 H_0} \int_0^{z_{max}} \frac{\mathcal{R}(z)}{(1+z)E(z)} \left\langle \frac{dE_{\text{gw}}}{df_s} \right\rangle_{f_s} dz}, \quad (\text{A22})$$

which yields Eq. (2) when using the definition of the critical density ρ_c .

B. SNR OF THE GWB AND PROJECTIONS FOR FUTURE DETECTORS

The optimal SNR of the GW energy density Ω_{gw} in a given detector network is given by (Allen & Romano 1999)

$$\langle \text{SNR} \rangle_{\text{opt}} = \sqrt{(\gamma \Omega_{\text{gw}} | \gamma \Omega_{\text{gw}})}, \quad (\text{B23})$$

where γ is the overlap reduction function and the inner product is defined as in Eq. (7). Therefore, we can write the SNR as

$$\langle \text{SNR} \rangle_{\text{opt}} = \sqrt{2T \left(\frac{3H_0^2}{10\pi^2} \right)^2 \int_0^\infty df \frac{\gamma^2 \Omega_{\text{gw}}^2}{f^6 P_1(f) P_2(f)}}, \quad (\text{B24})$$

and note how it scales with the Hubble constant ($\Omega_{\text{gw}} \sim H_0^{-3} \Rightarrow \text{SNR} \sim H_0^{-1}$) and with observing time ($\text{SNR} \sim \sqrt{T}$). From this scaling, it is clear that longer observing times increase the chances of detecting a GWB and that the value of H_0 impacts the time to detection (reinforcing the earlier point from Sec. 2 that a non-detection implies larger values of H_0). We can make projections for the time to detection in future detector networks as in Fig. 2. Note that as in the rest of this work, we are considering only the BBH contribution to Ω_{gw} , so our energy spectrum may be an underestimate, and these are thus conservative projections for the time to detection. Here, we pin the parameters to their mean values (Table 2) as obtained from Abbott et al. (2023a), and consider two values of H_0 (those from Aghanim et al. (2020); Riess et al. (2022)). We consider three different cases with the sensitivities predicted for advanced LIGO (aLIGO), A#, and Voyager. In all cases, we conservatively assume a detector network composed of LIGO-Hanford, LIGO-Livingston, and Virgo, all with the same sensitivity. The SNR of this detector network is

$$\langle \text{SNR} \rangle_{\text{net}} = \sqrt{\text{SNR}_{\text{HL}}^2 + \text{SNR}_{\text{HV}}^2 + \text{SNR}_{\text{LV}}^2}, \quad (\text{B25})$$

where the SNR between each pair of detectors is added in quadrature to obtain the total. With these estimates, we find the time to detection in aLIGO too long to be practical (on the order of centuries of observation needed for an

α	β	m_{\min}	m_{\max}	λ_g	μ_g	σ_g	δ_m	R	γ	κ	z_p	$\Omega_{m,0}$	w_0	H_0
3.4	1.08	5.08	86.85	0.04	33.73	3.56	4.83	17.975	2.7	2.9	1.9	0.3065	-1	67.4, 73

Table 2. The values of the parameters used for all SNR estimates in Appx B. All population parameters and mass model parameters are set to the mean value of the posterior distributions from (Abbott et al. 2023a), while the cosmological parameters are set by (Aghanim et al. 2020; Riess et al. 2022).

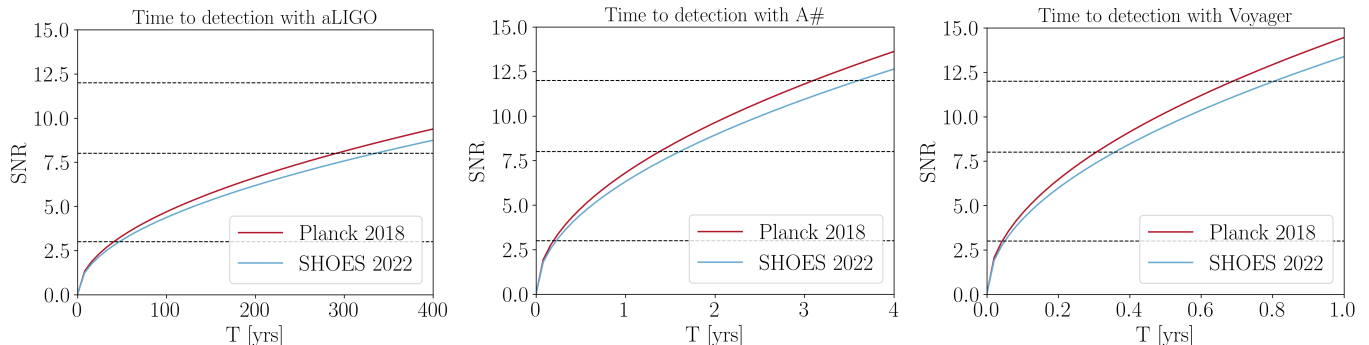


Figure 2. The time to detect a GWB with a detector network consisting of LIGO-Hanford, LIGO-Livingston, and Virgo with the sensitivity of aLIGO, A#, or voyager. In all plots, the dashed lines represent SNR values of three, eight, and twelve respectively, and results are shown for both the Planck (Aghanim et al. 2020) and SHOES (Riess et al. 2022) values of H_0 to give an example for how time to detection changes with H_0 . Note that the time to detection is very different across these different networks, so these plots have a different scaling on the x-axis.

SNR of eight). However, A# and Voyager are more promising, with both networks capable of detecting the GWB with the assumed properties within two years. The factor of ~ 10 improvement in sensitivity between aLIGO and A# is responsible for this dramatic improvement in time to detection.

The estimates in Fig. 2 were performed assuming specific values for each of the parameters, yet it is informative to consider how the SNR can change with different combinations of the parameters. Thus, Fig. 3 demonstrates the relation between two parameters at a time (with all other parameters held fixed at the values in Table 2), with SNR represented via a heatmap as function of cosmological parameters $\{H_0, \Omega_{m,0}, w_0\}$. Additional plots for the other parameters can be found in the supplemental materials. The contour lines represent SNR values of 8 and 20. These plots illustrate which regions of parameter space could be ruled out by a non-detection of the GWB, as any combination of parameters that corresponds to an SNR larger than eight (beyond the contour line) should have been measurable. The horizontal and vertical lines correspond to the mean values of the parameters listed in Table 2 and the H_0 measurements from Aghanim et al. (2020) and Riess et al. (2022), respectively, to give an idea of where we expect the GWB to be on these plots, given current data. Figure 3 explicitly shows the SNR in a network of A# detectors after one and two years to demonstrate the increase in SNR over time, but a movie illustrating the change in SNR over time is available in the supplemental materials. Analogously, Fig. 4 illustrates lines of constant SNR for these same parameters, but with multiple different networks observing for the same two-year period. Figure 4 is consistent with Fig. 2, demonstrating that after two years of observation, aLIGO would not confidently detect a GWB with these parameters, A# would measure it with $\text{SNR} \approx 8$, and Voyager would measure it with $\text{SNR} \approx 20$.

C. PARAMETER INFERENCE

We describe the population models used in our inference. We selected specific mass and redshift models in order to compare with previous results (Abbott et al. 2023a). For a description of the PowerLaw+Peak mass model, we refer to existing sources (Talbot & Thrane 2018; Collaboration et al. 2019; Talbot et al. 2024) and its implementation via equations B.10-12 in Mastrogiovanni et al. (2023). For the redshift model, we use a functional form of the Madau-Dickinson model Madau & Dickinson (2014) as parametrized in Callister et al. (2020):

$$\mathcal{R}(z) = R_0 [1 + (1 + z_p)^{-\gamma - \kappa}] \frac{(1 + z)^\gamma}{1 + \left(\frac{1+z}{1+z_p}\right)^{\gamma + \kappa}}. \quad (\text{C26})$$

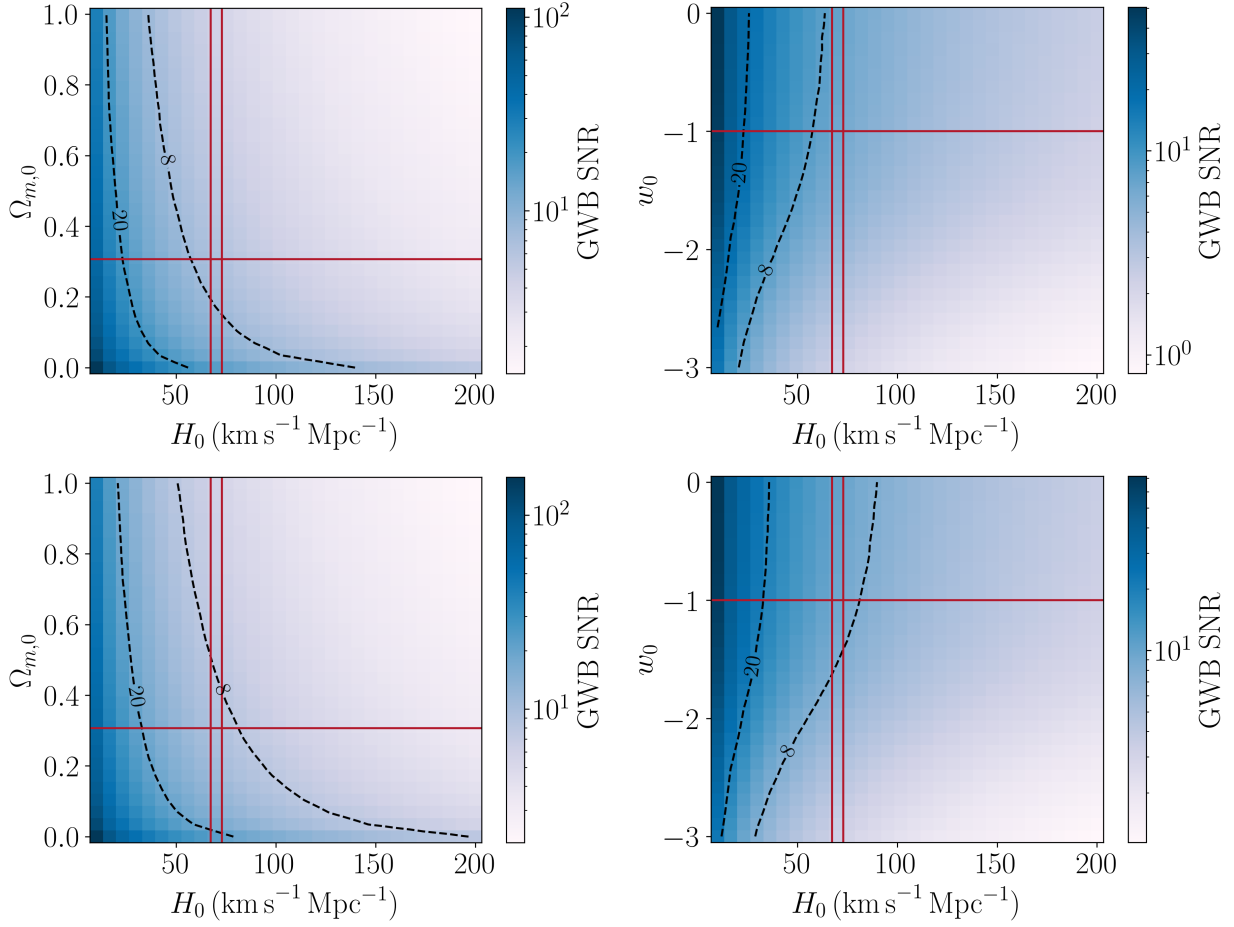


Figure 3. SNR of the GWB in a future detector network with A# sensitivity as a function of varying cosmological parameters. The upper plots are after one year of observation, while the lower plots are after two years of observation. Contour lines illustrate constant values of SNR=8 and SNR=20, while the red horizontal and vertical lines indicate the expected values (corresponding to those listed in Table 2) of these parameters. Observe that the region of parameter space that is detectable increases with increasing observing time and we expect the GWB to be detectable after two years.

Refer to Table 1 for descriptions the hyperparameters.

For all results of \mathcal{L}_{FG} , \mathcal{L}_{BG} , and $\mathcal{L}_{\text{joint}}$, we ensured convergence by checking consistency between results obtained using lower (2048) and higher (3072) counts of live points, as is conventional in nested sampling analysis. Additionally, we tested two different bandwidths for generating KDEs from the Abbott et al. (2023a) posteriors and obtained results consistent with each other.

To check consistency with previous results, the BBH spectral siren results of Abbott et al. (2023a) should be recovered, given that we adopted their population hyperparameter posteriors in our analysis. We note that within Fig. 1, the results of \mathcal{L}_{FG} are directly comparable to the results obtained via the BBH spectral siren method of Abbott et al. (2023a), whose median and 90% credible interval is reported as 67^{+91}_{-47} in their Table 4. We recover comparable results as 69.9^{+83}_{-50} .

C.1. Other parameter results

We show our inference results for the redshift model and cosmology parameters Fig. 5. We found that the mass hyperparameter constraints are effectively unchanged by the inclusion of the GWB, so those results are not shown here (see the supplemental material). Note that in general, measurements of most hyperparameters are not greatly altered by the inclusion of the GWB non-detection.

However, observe that the redshift model hyperparameters R_0 (the local merger rate) and γ (the exponent governing the lower-redshift merger rate, as in Eq. (C26)) have some marginal improvements, namely a tendency toward lower

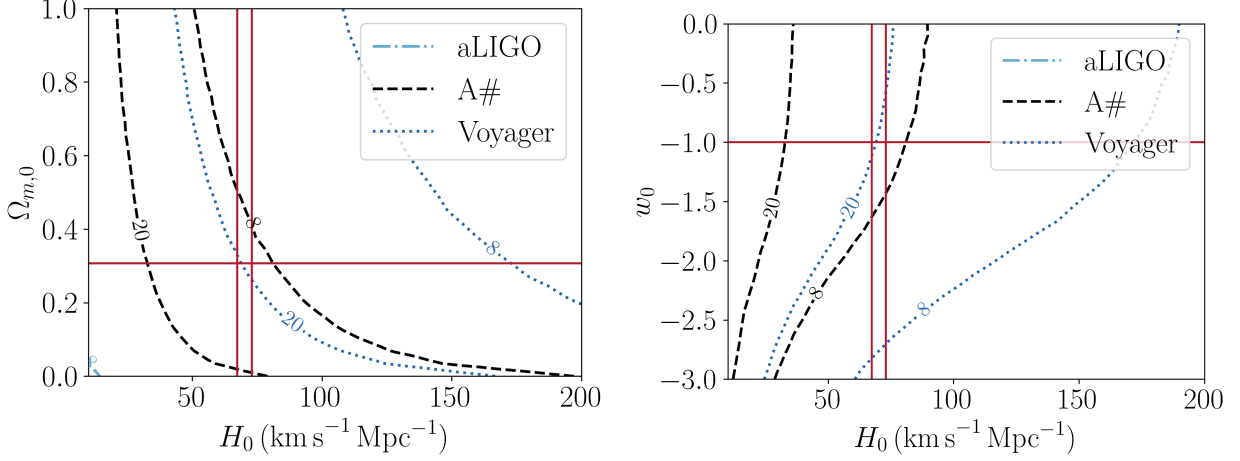


Figure 4. SNR of the GWB in future detector networks with aLIGO, A#, and Voyager sensitivity, as a function of varying cosmological parameters. These plots represent the SNR after two years of observation. Contour lines illustrate constant values of SNR=8 and SNR=20 for each network, while the red horizontal and vertical lines indicate the expected values (corresponding to those listed in Table 2) of these parameters. Note that there are no values of these parameters that would make the GWB measurable in aLIGO after only two years. For plots of the other parameters, see supplemental materials.

values. This is sensible given that the upper limit on Ω_{gw} will favor lower values of both the rate R_0 and γ since higher values of these hyperparameters implies more mergers, and thus a larger Ω_{gw} . There is hence some correlation between H_0 and these parameters, which agrees with the findings of Ferraiuolo et al. (2025).

REFERENCES

- Aasi, J., et al. 2015, *Classical and quantum gravity*, 32, 074001
- Abbott, B., et al. 2017, *Nature*, 551, 85
- Abbott, B. P., Abbott, R., Abbott, T. D., et al. 2016a, *Physical Review Letters*, 116, 131102, doi: [10.1103/PhysRevLett.116.131102](https://doi.org/10.1103/PhysRevLett.116.131102)
- Abbott, B. P., et al. 2016b, *Phys. Rev. Lett.*, 116, 131102, doi: [10.1103/PhysRevLett.116.131102](https://doi.org/10.1103/PhysRevLett.116.131102)
- . 2018, *Phys. Rev. Lett.*, 120, 091101, doi: [10.1103/PhysRevLett.120.091101](https://doi.org/10.1103/PhysRevLett.120.091101)
- Abbott, R., Abbott, T. D., Abraham, S., et al. 2021a, *Physical Review D*, 104, 022004, doi: [10.1103/PhysRevD.104.022004](https://doi.org/10.1103/PhysRevD.104.022004)
- Abbott, R., et al. 2021b, *Physical Review X*, 11, 021053
- Abbott, R., Abe, H., Acernese, F., et al. 2023a, *The Astrophysical Journal*, 949, 76, doi: [10.3847/1538-4357/ac74bb](https://doi.org/10.3847/1538-4357/ac74bb)
- Abbott, R., et al. 2023b, *Phys. Rev. X*, 13, 011048, doi: [10.1103/PhysRevX.13.011048](https://doi.org/10.1103/PhysRevX.13.011048)
- . 2023c, *Physical Review X*, 13, 041039
- Acernese, F., Agathos, M., Agatsuma, K., et al. 2014, *Classical and Quantum Gravity*, 32, 024001
- Agazie, G., Anumalapudi, A., Archibald, A. M., et al. 2023, *The Astrophysical Journal Letters*, 951, L8
- Aghanim, N., Akrami, Y., Ashdown, M., et al. 2020, *Astronomy & Astrophysics*, 641, A6
- Alam, S., Aubert, M., Avila, S., et al. 2021, *Physical Review D*, 103, 083533, doi: [10.1103/PhysRevD.103.083533](https://doi.org/10.1103/PhysRevD.103.083533)
- Allen, B., & Romano, J. D. 1999, *Physical Review D*, 59, 102001, doi: [10.1103/PhysRevD.59.102001](https://doi.org/10.1103/PhysRevD.59.102001)
- Ashton, G., et al. 2019, *Astrophys. J. Suppl.*, 241, 27, doi: [10.3847/1538-4365/ab06fc](https://doi.org/10.3847/1538-4365/ab06fc)
- Astropy Collaboration, Robitaille, T. P., Tollerud, E. J., et al. 2013, *A&A*, 558, A33, doi: [10.1051/0004-6361/201322068](https://doi.org/10.1051/0004-6361/201322068)
- Astropy Collaboration, Price-Whelan, A. M., Sipőcz, B. M., et al. 2018, *AJ*, 156, 123, doi: [10.3847/1538-3881/aabc4f](https://doi.org/10.3847/1538-3881/aabc4f)
- Astropy Collaboration, et al. 2022, *ApJ*, 935, 167, doi: [10.3847/1538-4357/ac7c74](https://doi.org/10.3847/1538-4357/ac7c74)
- Balkenhol, L., Dutcher, D., Mancini, A. S., et al. 2023, *Physical Review D*, 108, 023510, doi: [10.1103/PhysRevD.108.023510](https://doi.org/10.1103/PhysRevD.108.023510)
- Belczynski, K., Dominik, M., Bulik, T., et al. 2010, *The Astrophysical Journal Letters*, 715, L138
- Bera, S., Rana, D., More, S., & Bose, S. 2020, *The Astrophysical Journal*, 902, 79

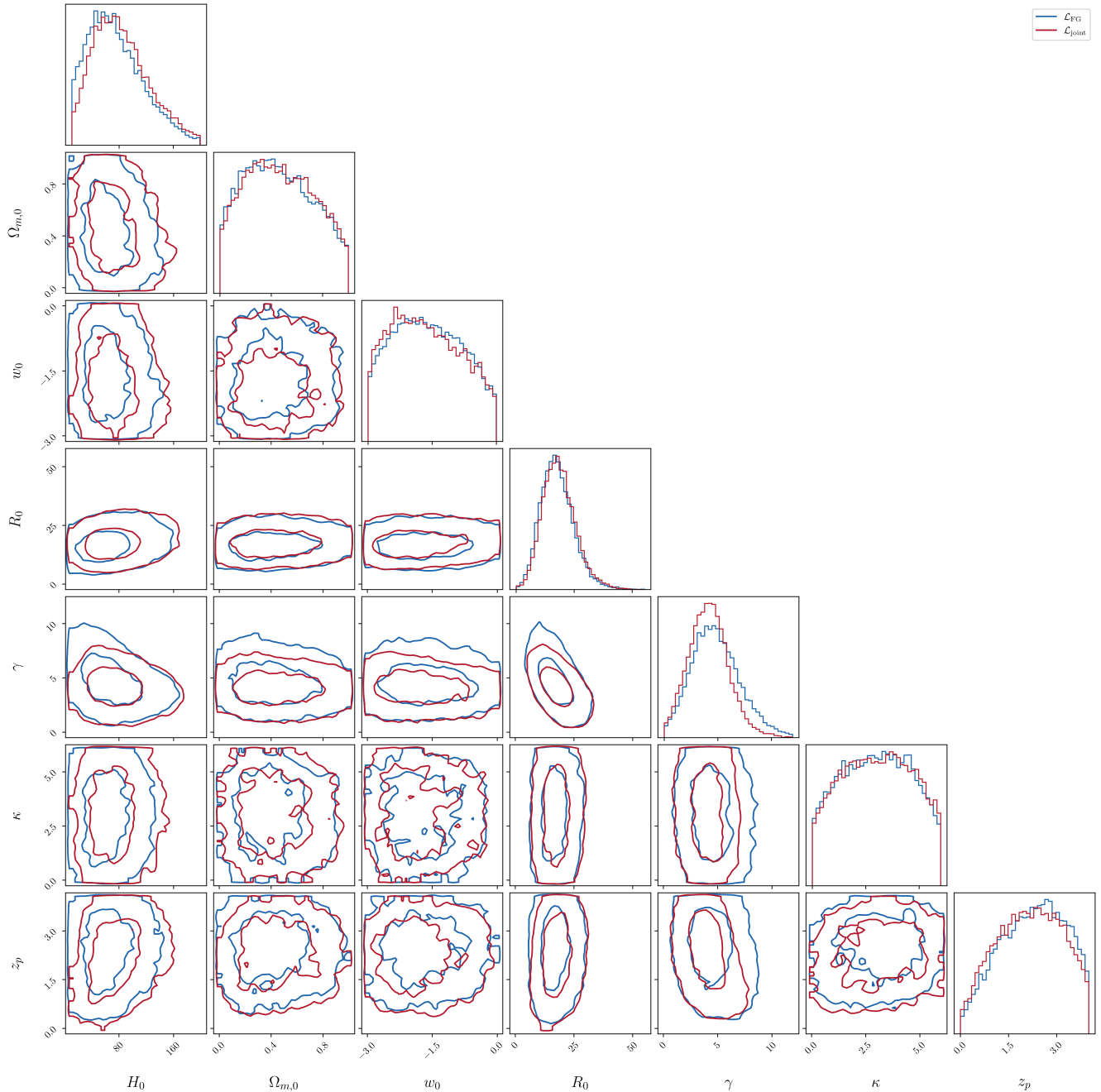


Figure 5. Redshift model hyperparameters, together with cosmological parameters, as inferred via the BBH spectral siren (\mathcal{L}_{bbh} , blue) and stochastic siren ($\mathcal{L}_{\text{joint}}$, red) methods. Observe that most hyperparameters do not demonstrate an improvement with the current non-detection of the BBH GWB, with the exception of R_0 and γ as elaborated in the main text.

Borhanian, S., Dhani, A., Gupta, A., Arun, K., & Sathyaprakash, B. 2020, *The Astrophysical Journal Letters*, 905, L28

Branchesi, M., et al. 2023, *JCAP*, 07, 068, doi: [10.1088/1475-7516/2023/07/068](https://doi.org/10.1088/1475-7516/2023/07/068)

Brout, D., Scolnic, D., Popovic, B., et al. 2022, *The Astrophysical Journal*, 938, 110, doi: [10.3847/1538-4357/ac8e04](https://doi.org/10.3847/1538-4357/ac8e04)

Buscicchio, R., Ain, A., Ballelli, M., Cella, G., & Patricelli, B. 2023, *Phys. Rev. D*, 107, 063027, doi: [10.1103/PhysRevD.107.063027](https://doi.org/10.1103/PhysRevD.107.063027)

- Callister, T., Fishbach, M., Holz, D. E., & Farr, W. M. 2020, *The Astrophysical Journal*, 896, L32, doi: [10.3847/2041-8213/ab9743](https://doi.org/10.3847/2041-8213/ab9743)
- Callister, T., Biscoveanu, A. S., Christensen, N., et al. 2017, *Physical Review X*, 7, 041058, doi: [10.1103/PhysRevX.7.041058](https://doi.org/10.1103/PhysRevX.7.041058)
- Caprini, C., & Figueroa, D. G. 2018, *Classical and Quantum Gravity*, 35, 163001
- Chatterjee, D., Hegade KR, A., Holder, G., et al. 2021, *Physical Review D*, 104, 083528
- Chen, H.-Y., Fishbach, M., & Holz, D. E. 2018, *Nature*, 562, 545, doi: [10.1038/s41586-018-0606-0](https://doi.org/10.1038/s41586-018-0606-0)
- Chen, H.-Y., Haster, C.-J., Vitale, S., Farr, W. M., & Isi, M. 2022, *Monthly Notices of the Royal Astronomical Society*, 513, 2152
- Chernoff, D. F., & Finn, L. S. 1993, arXiv preprint gr-qc/9304020
- Chowdhury, S. R., & Khlopov, M. 2024, *Phys. Rev. D*, 110, 063037, doi: [10.1103/PhysRevD.110.063037](https://doi.org/10.1103/PhysRevD.110.063037)
- Christensen, N. 1992, *Phys. Rev. D*, 46, 5250, doi: [10.1103/PhysRevD.46.5250](https://doi.org/10.1103/PhysRevD.46.5250)
- Collaboration, DESI., Adame, A. G., Aguilar, J., et al. 2024, DESI 2024 VI: Cosmological Constraints from the Measurements of Baryon Acoustic Oscillations, arXiv, doi: [10.48550/arXiv.2404.03002](https://doi.org/10.48550/arXiv.2404.03002)
- Collaboration, T. L. S., the Virgo Collaboration, Abbott, B. P., et al. 2019, *The Astrophysical Journal*, 882, L24, doi: [10.3847/2041-8213/ab3800](https://doi.org/10.3847/2041-8213/ab3800)
- Collette, A. 2013, Python and HDF5: unlocking scientific data ("O'Reilly Media, Inc.")
- Dalal, N., Holz, D. E., Hughes, S. A., & Jain, B. 2006, *Physical Review D*, 74, 063006, doi: [10.1103/PhysRevD.74.063006](https://doi.org/10.1103/PhysRevD.74.063006)
- Del Pozzo, W. 2012, *Physical Review D—Particles, Fields, Gravitation, and Cosmology*, 86, 043011
- Di Valentino, E., Mena, O., Pan, S., et al. 2021, *Classical and Quantum Gravity*, 38, 153001
- Dodelson, S., & Schmidt, F. 2003, *Modern cosmology* (Elsevier)
- Drasco, S., & Flanagan, É. É. 2003, *PhRvD*, 67, 082003, doi: [10.1103/PhysRevD.67.082003](https://doi.org/10.1103/PhysRevD.67.082003)
- Easter, R., & Lim, E. A. 2006, *Journal of Cosmology and Astroparticle Physics*, 2006, 010
- Evans, M., et al. 2021, doi: [10.48550/arXiv.2109.09882](https://doi.org/10.48550/arXiv.2109.09882)
- . 2023. <https://arxiv.org/abs/2306.13745>
- Ezquiaga, J. M., & Holz, D. E. 2021, *The Astrophysical Journal Letters*, 909, L23
- . 2022, *Physical Review Letters*, 129, 061102
- Farr, W. M., Fishbach, M., Ye, J., & Holz, D. E. 2019, *The Astrophysical Journal Letters*, 883, L42
- Ferraiuolo, S., Mastrogiovanni, S., Kajfasz, E., & Escoffier, S. 2025, *in preparation*.
- Ferrari, V., Matarrese, S., & Schneider, R. 1999a, *Monthly Notices of the Royal Astronomical Society*, 303, 258, doi: [10.1046/j.1365-8711.1999.02207.x](https://doi.org/10.1046/j.1365-8711.1999.02207.x)
- . 1999b, *Mon. Not. Roy. Astron. Soc.*, 303, 247, doi: [10.1046/j.1365-8711.1999.02194.x](https://doi.org/10.1046/j.1365-8711.1999.02194.x)
- Finke, A., Foffa, S., Iacovelli, F., Maggiore, M., & Mancarella, M. 2021, *Journal of Cosmology and Astroparticle Physics*, 2021, 026
- Fischbach, M., Davis, D., & Renzini, A. 2021, Investigating data quality metrics for stochastic gravitational-wave detection. <https://dcc-backup.ligo.org/public/0176/T2100203/001/Fischbach.First.Interim.Report.pdf>
- Fishbach, M., Gray, R., Hernandez, I. M., et al. 2019, *The Astrophysical Journal Letters*, 871, L13
- Flanagan, E. E. 1993, *Phys. Rev. D*, 48, 2389, doi: [10.1103/PhysRevD.48.2389](https://doi.org/10.1103/PhysRevD.48.2389)
- Flanagan, É. É., & Hughes, S. A. 1998, *Physical Review D*, 57, 4535
- Freedman, W. L. 2021, *The Astrophysical Journal*, 919, 16, doi: [10.3847/1538-4357/ac0e95](https://doi.org/10.3847/1538-4357/ac0e95)
- Gallegos-Garcia, M., Berry, C. P., Marchant, P., & Kalogera, V. 2021, *The Astrophysical Journal*, 922, 110
- Gray, R., Hernandez, I. M., Qi, H., et al. 2020, *Physical Review D*, 101, 122001
- Gray, R., Beirnaert, F., Karathanasis, C., et al. 2023, *Journal of Cosmology and Astroparticle Physics*, 2023, 023
- Harris, C. R., et al. 2020, *Nature*, 585, 357
- Hogg, D. W. 1999, arXiv preprint astro-ph/9905116
- Holz, D. E., & Hughes, S. A. 2005, *The Astrophysical Journal*, 629, 15, doi: [10.1086/431341](https://doi.org/10.1086/431341)
- Hunter, J. D. 2007, *Computing in science & engineering*, 9, 90
- Jimenez, R., Cimatti, A., Verde, L., Moresco, M., & Wandelt, B. 2019, *Journal of Cosmology and Astroparticle Physics*, 2019, 043, doi: [10.1088/1475-7516/2019/03/043](https://doi.org/10.1088/1475-7516/2019/03/043)
- Kamionkowski, M., & Riess, A. G. 2022, *The Hubble Tension and Early Dark Energy*, arXiv. <http://ascl.net/2211.04492>
- Kibble, T. W. 1976, *Journal of Physics A: Mathematical and General*, 9, 1387
- Kushnir, D., Zaldarriaga, M., Kollmeier, J. A., & Waldman, R. 2016, *Monthly Notices of The Royal Astronomical Society*, 462, 844
- Lalleman, M., Turbang, K., Callister, T., & van Remortel, N. 2025. <https://arxiv.org/abs/2501.10295>

- Linder, E. V. 2003, *Physical Review Letters*, 90, 091301, doi: [10.1103/PhysRevLett.90.091301](https://doi.org/10.1103/PhysRevLett.90.091301)
- Macaulay, E., Nichol, R. C., Bacon, D., et al. 2019, *Monthly Notices of the Royal Astronomical Society*, 486, 2184, doi: [10.1093/mnras/stz978](https://doi.org/10.1093/mnras/stz978)
- MacLeod, C. L., & Hogan, C. J. 2008, *Physical Review D—Particles, Fields, Gravitation, and Cosmology*, 77, 043512
- Madau, P., & Dickinson, M. 2014, *ARA&A*, 52, 415, doi: [10.1146/annurev-astro-081811-125615](https://doi.org/10.1146/annurev-astro-081811-125615)
- Madau, P., & Dickinson, M. 2014, *Annual Review of Astronomy and Astrophysics*, 52, 415
- Maggiore, M., et al. 2020, *Journal of Cosmology and Astroparticle Physics*, 2020, 050, doi: [10.1088/1475-7516/2020/03/050](https://doi.org/10.1088/1475-7516/2020/03/050)
- Mali, U., & Essick, R. 2025, *Astrophys. J.*, 980, 85, doi: [10.3847/1538-4357/ad9de7](https://doi.org/10.3847/1538-4357/ad9de7)
- Mandel, I., Farr, W. M., & Gair, J. R. 2019, *Mon. Not. Roy. Astron. Soc.*, 486, 1086, doi: [10.1093/mnras/stz896](https://doi.org/10.1093/mnras/stz896)
- Mandic, V., Thrane, E., Giampanis, S., & Regimbau, T. 2012, *Physical review letters*, 109, 171102
- Marassi, S., Schneider, R., Corvino, G., Ferrari, V., & Zwart, S. P. 2011, *Physical Review D—Particles, Fields, Gravitation, and Cosmology*, 84, 124037
- Mastrogiovanni, S., Pierra, G., Perriès, S., et al. 2023, *ICAROGW: A Python Package for Inference of Astrophysical Population Properties of Noisy, Heterogeneous and Incomplete Observations*, arXiv. <https://arxiv.org/abs/2305.17973>
- Messenger, C., & Read, J. 2012, *Physical review letters*, 108, 091101
- Mukherjee, S., Krolewski, A., Wandelt, B. D., & Silk, J. 2024, *The Astrophysical Journal*, 975, 189
- Mukherjee, S., Wandelt, B. D., Nissanke, S. M., & Silvestri, A. 2021, *Physical Review D*, 103, 043520
- Mukherjee, S., Wandelt, B. D., & Silk, J. 2020, *Monthly Notices of the Royal Astronomical Society*, 494, 1956
- Nair, R., Bose, S., & Saini, T. D. 2018, *Physical Review D*, 98, 023502
- Nishizawa, A. 2017, *Physical Review D*, 96, 101303
- Nissanke, S., Holz, D. E., Dalal, N., et al. 2013, arXiv preprint arXiv:1307.2638
- Oguri, M. 2016, *Physical Review D*, 93, 083511
- Palmese, A., Devicente, J., Pereira, M., et al. 2020, *The Astrophysical Journal Letters*, 900, L33
- Punturo, M., et al. 2010, *Classical and Quantum Gravity*, 27, 194002, doi: [10.1088/0264-9381/27/19/194002](https://doi.org/10.1088/0264-9381/27/19/194002)
- Regimbau, T. 2011, *Research in Astronomy and Astrophysics*, 11, 369, doi: [10.1088/1674-4527/11/4/001](https://doi.org/10.1088/1674-4527/11/4/001)
- Regimbau, T., & Mandic, V. 2008, *Classical and Quantum Gravity*, 25, 184018
- Reitze, D., et al. 2019, arXiv preprint arXiv:1907.04833, doi: [10.48550/arXiv.1907.04833](https://doi.org/10.48550/arXiv.1907.04833)
- Renzini, A. I., & Golomb, J. 2024, arXiv preprint arXiv:2407.03742
- Renzini, A. I., Goncharov, B., Jenkins, A. C., & Meyers, P. M. 2022, *Stochastic Gravitational-Wave Backgrounds: Current Detection Efforts and Future Prospects*, arXiv. <https://arxiv.org/abs/2202.00178>
- Renzini, A. I., Romero-Rodríguez, A., Talbot, C., et al. 2023, *The Astrophysical Journal*, 952, 25
- Riess, A. G., Casertano, S., Yuan, W., Macri, L. M., & Scolnic, D. 2019, *The Astrophysical Journal*, 876, 85, doi: [10.3847/1538-4357/ab1422](https://doi.org/10.3847/1538-4357/ab1422)
- Riess, A. G., Filippenko, A. V., Challis, P., et al. 1998, *The astronomical journal*, 116, 1009
- Riess, A. G., et al. 2022, *Astrophys. J. Lett.*, 934, L7, doi: [10.3847/2041-8213/ac5c5b](https://doi.org/10.3847/2041-8213/ac5c5b)
- Rinaldi, S., Del Pozzo, W., Mapelli, M., Lorenzo-Medina, A., & Dent, T. 2024, *Astronomy & Astrophysics*, 684, A204
- Romano, J. D., & Cornish, N. J. 2017, *Living Reviews in Relativity*, 20, 2, doi: [10.1007/s41114-017-0004-1](https://doi.org/10.1007/s41114-017-0004-1)
- Rosado, P. A. 2011, *Physical Review D—Particles, Fields, Gravitation, and Cosmology*, 84, 084004
- Schutz, B. F. 1986, *Nature*, 323, 310, doi: [10.1038/323310a0](https://doi.org/10.1038/323310a0)
- Skilling, J. 2004, *Bayesian inference and maximum entropy methods in science and engineering*, 735, 395
- . 2006
- Smith, R., & Thrane, E. 2018, *Physical Review X*, 8, 021019, doi: [10.1103/PhysRevX.8.021019](https://doi.org/10.1103/PhysRevX.8.021019)
- Soares-Santos, M., et al. 2019, *The Astrophysical Journal Letters*, 876, L7, doi: [10.3847/2041-8213/ab14f1](https://doi.org/10.3847/2041-8213/ab14f1)
- Somiya, K., & Collaboration, K. 2012, *Classical and Quantum Gravity*, 29, 124007
- Speagle, J. S. 2020, *Mon. Not. Roy. Astron. Soc.*, 493, 3132, doi: [10.1093/mnras/staa278](https://doi.org/10.1093/mnras/staa278)
- Starobinskii, A. 1979, *JETP Letters*, 30, 682
- Suyu, S., Marshall, P., Auger, M., et al. 2010, *The Astrophysical Journal*, 711, 201
- Talbot, C., Farah, A., Galaudage, S., Golomb, J., & Tong, H. 2024, arXiv preprint arXiv:2409.14143
- Talbot, C., & Thrane, E. 2018, *ApJ*, 856, 173, doi: [10.3847/1538-4357/aab34c](https://doi.org/10.3847/1538-4357/aab34c)
- Taylor, S. R., & Gair, J. R. 2012, *Physical Review D—Particles, Fields, Gravitation, and Cosmology*, 86, 023502

- Taylor, S. R., Gair, J. R., & Mandel, I. 2012, *Physical Review D—Particles, Fields, Gravitation, and Cosmology*, 85, 023535
- Taylor, S. R., & Gerosa, D. 2018, *Phys. Rev. D*, 98, 083017, doi: [10.1103/PhysRevD.98.083017](https://doi.org/10.1103/PhysRevD.98.083017)
- Thorne, K. S. 1987, *Three hundred years of gravitation*, 330
- Tornamenti, S., Mapelli, M., Périgois, C., et al. 2024, *Astronomy & Astrophysics*, 688, A148
- Turbang, K., Lalleman, M., Callister, T. A., & van Remortel, N. 2024, *The Astrophysical Journal*, 967, 142
- Van Son, L., De Mink, S., Callister, T., et al. 2022, *The Astrophysical Journal*, 931, 17
- Virtanen, P., et al. 2020, *Nature methods*, 17, 261
- Vitale, S., & Chen, H.-Y. 2018, *Physical review letters*, 121, 021303
- Vitale, S., Gerosa, D., Farr, W. M., & Taylor, S. R. 2022, doi: [10.1007/978-981-15-4702-7_45-1](https://doi.org/10.1007/978-981-15-4702-7_45-1)
- Wong, K. C., Suyu, S. H., Chen, G. C.-F., et al. 2020, *Monthly Notices of the Royal Astronomical Society*, 498, 1420, doi: [10.1093/mnras/stz3094](https://doi.org/10.1093/mnras/stz3094)
- Wu, C., Mandic, V., & Regimbau, T. 2012, *Physical Review D—Particles, Fields, Gravitation, and Cosmology*, 85, 104024
- You, Z.-Q., Zhu, X.-J., Ashton, G., Thrane, E., & Zhu, Z.-H. 2021, *The Astrophysical Journal*, 908, 215
- Yu, J., Wang, Y., Zhao, W., & Lu, Y. 2020, *Monthly Notices of the Royal Astronomical Society*, 498, 1786
- Zhu, X.-J., Howell, E., Regimbau, T., Blair, D., & Zhu, Z.-H. 2011, *The Astrophysical Journal*, 739, 86
- Zhu, X.-J., Howell, E. J., Blair, D. G., & Zhu, Z.-H. 2013, *Monthly Notices of the Royal Astronomical Society*, 431, 882, doi: [10.1093/mnras/stt207](https://doi.org/10.1093/mnras/stt207)